CFD98, the 6th Annual Conference of the CFD Society of Canada, Quebec City, PQ, 7-9 June, 1998
Awarded 1st Prize, Student Paper Competition

MODELLING THE FINGERING OF IMPACTING DROPLETS

M. Bussmann*, S.D. Aziz†, J. Mostaghimi‡ and S. Chandra§
Department of Mechanical and Industrial Engineering
University of Toronto

ABSTRACT

A numerical model has been developed to simulate the fingering and splashing behaviour associated with the vigorous impact of a droplet against a solid surface. The model is a three-dimensionalization and improvement of the two-dimensional RIPPLE [1], an Eulerian fixed-grid control volume-based free surface code. Surface tension is treated continuously, as a force acting on fluid near the interface, and the model incorporates Youngs' piecewise-linear volume tracking algorithm to follow the free surface. Results are presented of three simulations of a liquid droplet impacting a surface at different velocities, which demonstrate behaviour ranging from a slight asymmetry to the formation of fingers and finally to the onset of splashing. Results are compared with experiment, and demonstrate good agreement.

INTRODUCTION

The impact of a droplet against a solid surface is a common occurrence in many processes including, for example, ink jet printing, thermal spraying and spray cooling and forming. If an impact is sufficiently vigorous, an instability forms at the fluid rim shortly after impact, which may lead to an outward growth of fingers. If the fingers grow sufficiently long, they too become unstable and break off to form so-called satellite droplets, which define droplet splashing. Understanding such behaviour, and predicting the onset of splashing and the size and number of droplets, is important for modelling processes such as those mentioned.

Studies of such behaviour are few, yet date back to the beautiful illustrations of Worthington [2]. More recently, Allen [3] proposed a simple model to predict the number of fingers, based on an application of Rayleigh-Taylor instability theory to the outward spread of fluid. And Marmanis and Thoroddsen [4] related the number of fingers to a single dimensionless parameter incorporating inertial, surface tension and viscous effects. Predictions in each case demonstrated reasonable agreement with experiment. Regarding the onset of splashing, Stow and Hadfield [5] and Mundo et al. [6] related experimental observations to a critical value of a parameter similar to that of Marmanis and Thoroddsen [4].

Yet despite these results, there is no adequate theory to explain the mechanism which initiates the instability at the droplet rim. Towards that end, this paper presents a numerical model of droplet impact to examine fingering and splashing. Where previous droplet impact models have invoked an assumption of axisymmetry (e.g. [7, 8]) which precludes modelling fingering and splashing, the model presented here is fully three-dimensional. The equations and discretization are presented, followed by the results of three simulations, which are compared with corresponding photographs.

METHODOLOGY

Equations

Model formulation begins with the assumption that the surrounding gas phase exerts negligible influence on the liquid during impact. This implies that surface viscous stresses are negligible, and that only the liquid phase flowfield need be solved, subject to boundary conditions at the free surface. For an incompressible, Newtonian fluid with constant properties, the equations of conservation of mass and momentum are:

$$\nabla \cdot \vec{V} = 0 \tag{1}$$

$$\frac{\partial \vec{V}}{\partial t} + \nabla \cdot (\vec{V}\vec{V}) = -\frac{1}{\rho}\nabla p + \frac{\mu}{\rho}\nabla^2 \vec{V} + \frac{1}{\rho}\vec{F}_b \tag{2}$$

*bussmann@mie.utoronto.ca
†aziz@mie.utoronto.ca
‡mostag@mie.utoronto.ca
§chandra@mie.utoronto.ca

$\vec{V}$ represents velocity, p pressure, ρ density, μ viscosity, and $\vec{F}_b$ any body forces acting on the fluid.

Droplet splashing involves severe fluid deformation, and so the model employs a volume tracking algorithm to follow the free surface, where fluid volume is represented by a scalar f, defined as:

$$f = \begin{cases} 1 & \text{within the liquid phase} \\ 0 & \text{without} \end{cases} \tag{3}$$

Since f is a Lagrangian invariant, it satisfies:

$$\frac{\partial f}{\partial t} + (\vec{V} \cdot \nabla) f = 0 \tag{4}$$

Finally, with surface viscous stresses assumed negligible, the surface stress condition reduces to Laplace's equation for the surface tension-induced pressure jump Δp_s across the interface:

$$\Delta p_s = \gamma \kappa \tag{5}$$

γ represents the surface tension coefficient and κ the total curvature. Rather than impose Equation 5 as a boundary condition, surface tension is reformulated as an equivalent volume force $\vec{F}_{ST}$, as proposed by Brackbill et al. [9]:

$$\vec{F}_{ST}(\vec{x}) = \gamma \int_S \kappa(\vec{y})\, \hat{n}(\vec{y})\, \delta(\vec{x} - \vec{y})\, d\vec{y} \tag{6}$$

$\hat{n}$ represents an inward unit normal to the interface and δ the Dirac delta function, and the integration is performed over some area of free surface S. κ and $\hat{n}$ may be expressed in terms of f:

$$\kappa = -\nabla \cdot \hat{n} \tag{7}$$

$$\hat{n} = \frac{\nabla f}{|\nabla f|} \tag{8}$$

Formulated in this way, surface tension is then incorporated into Equation 2 via $\vec{F}_b$.

Boundary conditions at the solid surface are a no-slip, zero pressure gradient condition. At the free surface, velocity boundary conditions reflect the zero shear stress condition subject to the continuity constraint. Pressure at the free surface is set to zero since surface tension has been accounted for in Equation 2. And finally, a contact angle θ is specified at the contact line, at which the free surface meets the solid surface, to close Equation 6.

Discretization

The model which is presented here began as a three-dimensionalization of the two-dimensional RIPPLE code [1]. Parts of the discretization remain similar, and are presented here quickly. The significant differences relate to the treatment of surface tension and volume tracking, and are presented separately.

Equations 1, 2, 4 and 6 are discretized on a Cartesian grid, with velocities specified at the centre of cell faces and pressure at each cell centre.

f is integrated over each cell volume Ω_{ijk} to yield a discrete volume fraction f_{ijk}:

$$f_{ijk} = \frac{1}{\Omega_{ijk}} \int_{\Omega_{ijk}} f\, d\Omega \tag{9}$$

$f_{ijk} = 1$ if a cell is filled with liquid, $f_{ijk} = 0$ if a cell is empty, and $0 < f_{ijk} < 1$ if a cell contains a portion of the interface, deemed an "interface cell."

Equations 1 and 2 are solved with a two-step projection method, in which a time discretization of the momentum equation is divided into two steps:

$$\frac{\tilde{V} - \vec{V}^n}{\Delta t} = \nabla \cdot (\vec{V}\vec{V})^n + \frac{\mu}{\rho^n} \nabla^2 \vec{V}^n + \frac{1}{\rho^n} \vec{F}_b^n \tag{10}$$

$$\frac{\vec{V}^{n+1} - \tilde{V}}{\Delta t} = -\frac{1}{\rho^n} \nabla p^{n+1} \tag{11}$$

In the first step, Equation 10, an interim velocity $\tilde{V}$ is computed explicitly from convective, viscous and body force accelerations of the known field $\vec{V}^n$ for a timestep Δt. In the second step, $\tilde{V}$ is projected onto a divergence-free velocity field; combining Equation 11 with Equation 1 yields a Poisson equation for pressure:

$$\nabla \cdot \left(\frac{1}{\rho^n} \nabla p^{n+1}\right) = \frac{1}{\Delta t} \nabla \cdot \vec{\tilde{V}} \tag{12}$$

Note that although the fluid is assumed to be incompressible, the density is retained within the divergence operator to allow for the evaluation of non-zero density gradients across the liquid free surface.

The viscous and pressure terms of Equations 10 and 12 are discretized with centred difference approximations, while the convective term is treated with the conservative scheme of van Leer [10].

Surface Tension

Discretization of Equation 6 begins with replacing δ with a finite kernel δ_ϵ, to yield a surface tension force which applies to volume within a distance ϵ of the interface:

$$\vec{F}_{ST}(\vec{x}) \approx \gamma \int_S \kappa(\vec{y})\, \hat{n}(\vec{y})\, \delta_\epsilon(\vec{x} - \vec{y})\, d\vec{y} \tag{13}$$

Equation 13 is then treated as follows. A cell-centred surface tension force is evaluated for each interface cell:

$$\vec{F}_{ST_{ijk}} = \gamma \kappa_{ijk} \frac{A_{ijk}}{\Omega_{ijk}} \hat{n}_{ijk} \tag{14}$$

where A_{ijk} is the free surface area contained within the cell (the area of the planar interface reconstructed by the f advection algorithm, presented later), and κ_{ijk} and $\hat{n}_{ijk}$ are the cell-centred curvature and unit normal, respectively. Setting aside the evaluation of these quantities for a moment, $\vec{F}_{ST_{ijk}}$ is then convolved with δ_ϵ to obtain a smoothed force field $\tilde{F}_{ST_{ijk}}$:

$$\tilde{F}_{ST_{ijk}} = \sum_{ijk} \vec{F}_{ST_{ijk}} g_{ijk} \int_{\Omega_{ijk}} \delta_\epsilon(\vec{y} - \vec{x}_{ijk})\, d\vec{y} \qquad (15)$$

where δ_ϵ is integrated from about the cell centre $\vec{x}_{ijk}$. g_{ijk} is a weighting function defined by:

$$g_{ijk} = \frac{f_{ijk}}{\overline{f}} \qquad (16)$$

where $\overline{f} = 1/2$ represents the average value of f, which transforms the volume force into a body force irrespective of density.

The particular δ_ϵ chosen for the model is a radially-symmetric variation of a kernel proposed by Peskin [11]:

$$\delta_\epsilon(r) = \begin{cases} (1 + \cos(\pi r/\epsilon))\,/c & r \le \epsilon \\ 0 & r > \epsilon \end{cases} \qquad (17)$$

where c normalizes the kernel:

$$c = \frac{4}{3}\epsilon^3(\pi^2 - 6)/\pi \qquad (18)$$

The reason for modifying Peskin's kernel is found in work by Aleinov and Puckett [12] which demonstrates that radial symmetry is an attractive attribute of δ_ϵ. Good results have been obtained by limiting the spread radius ϵ to within the immediate neighbouring cells (a 3x3x3 stencil), which implies that $\epsilon = \frac{3}{2}\Delta x$ for a square grid.

Returning now to the evaluation of $\hat{n}_{ijk}$ and κ_{ijk}, the approach implemented borrows from the kernel-based approach to evaluating $\vec{F}_{ST}$. Evaluating ∇f with simple difference approximations of f_{ijk} yields poor estimates of $\hat{n}_{ijk}$, since the interface is nearly discontinuous. Instead, much better estimates result from evaluating the gradient of a smoothed field $\tilde{f}_{ijk}$, obtained by convolving f_{ijk} with δ_ϵ. In practice, the same kernel and the same spread radius are used for $\tilde{f}_{ijk}$ as for $\tilde{F}_{ST_{ijk}}$. Unit normals are obtained first at cell vertices, from which the κ_{ijk} are evaluted via a simple difference approximation to $-\nabla \cdot \hat{n}$. $\hat{n}_{ijk}$ are then obtained by averaging the vertex normals.

Volume Tracking

Since f_{ijk} is an integrated value, and in order to maintain a sharp interface (limited to one or two cells), the discretization of Equation 4 requires special treatment. Various schemes exist, many of which are geometric rather than algebraic, and which consist essentially of two steps: a reconstruction of the interface followed by a geometric evaluation of fluxes across cell faces.

The algorithm implemented in this model is the three-dimensional scheme of Youngs [13]. The interface is reconstructed by locating a three- to six-sided plane within each interface cell, corresponding exactly to f_{ijk} and $\hat{n}_{ijk}$. The number of sides equals the number of cell faces intersected. Note that the reconstruction does not require that adjacent interface planes be contiguous. The position of the interface and the velocities at the cell faces are then used to determine the fluid fluxes across each face during the timestep. Fluxes are evaluated one dimension at a time, followed by an interim interface reconstruction. Directional bias is minimized by alternating the order of advection from one timestep to the next.

RESULTS

Figures 1-3 illustrate the results of three simulations of the impact of a 2.7 mm diameter molten tin droplet onto a polished stainless steel surface at 1, 2 and 3 m/s. Figures 1 and 2 also present corresponding photographs, obtained with the experimental technique presented by Pasandideh-Fard et al. [14]. Note that the surface temperature was maintained at above the melting point of tin (232^oC), to render the impact isothermal.

Each of the simulations was run on a square grid, with resolution ranging from 50 to 64 cells per initial droplet diameter. In each case only one quarter of a droplet was considered, with symmetry conditions applied at the appropriate mesh boundaries. This was done to save on run time, and does not reflect any real symmetry. Rather, since the equations are discretized on a Cartesian grid, results of an impact normal to a solid surface are symmetrical in each of the four quadrants about the point of impact. This of course implies that fingering behaviour cannot be resolved beyond a multiple of four, as can be seen from examination of Figures 1-3. A relatively constant contact angle $\theta \approx 140^o$ was measured from photographs similar to those presented here, and this value imposed as the boundary condition at the contact line.

Regarding convergence, results of Figures 1 and 2 changed inappreciably with further grid refinement, and are deemed to have converged. The same cannot be said of the results of Figure 3, where the fingering behaviour evolved slowly with grid refinement even on the finest grid. The results are included here only

to demonstrate the capability of the model. Futher refinement is planned as computational resources become available. Each of the simulations ran for several days on a SGI Indigo 2 workstation.

The results of Figures 1-3 were obtained without "forcing" the instabilities. Unlike simulations of simple configurations of the Rayleigh-Taylor instability (e.g. [15, 16]), for example, where the interface between two fluids is initially at rest and must be perturbed to initiate motion, the instabilities presented here result only from the model discretization. In particular, during early stages of the simulations, inertial effects dominate over surface tension and viscous effects. Figures 1 and 2 in particular reveal a slight tendency for a droplet to spread preferentially along gridlines rather than diagonally across the mesh, resulting in the formation of lobes in Figure 1 and fingers in Figure 2. Simulations of less vigorous impacts remain much more symmetrical about the point of impact.

The results of Figure 1 demonstrate good agreement with the photographs, from the initial spread of fluid through to surface-tension induced recoil. In fact, simulation results beyond those presented here accurately predict the fluid bouncing off of the surface, and the pinch-off of a small droplet. The results of Figure 2 are somewhat less accurate, as the model predicts only eight of the 14 fingers which form during the outward spread of fluid. However, agreement is surprisingly good at 7 ms, when both simulation and experiment predict the recoil of eight fingers. As mentioned, the results of Figure 3 are preliminary, but demonstrate the capability of the model. Note that the results of Figure 3, and particularly at 1.6 ms, nonetheless predict the roughly 30 fingers observed experimentally. The biggest difference between simulation and experiment is the time to splashing: simulation results predict the premature formation and break off of fingers, corresponding to an underresolution of such features by the grid.

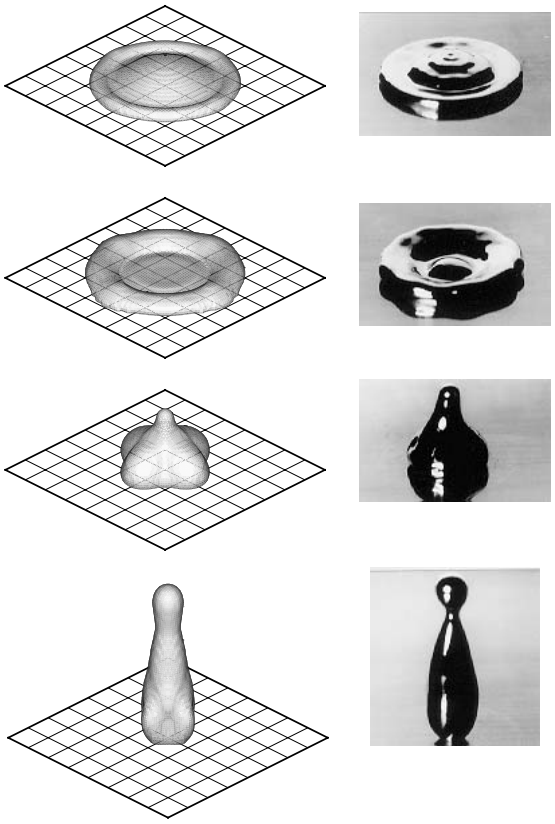

Figure 1: Simulation views and photographs of a 2.7 mm tin droplet impacting at 1 m/s. Results presented at 2, 5, 8 and 12 ms following impact.

CONCLUSIONS

A three-dimensional, Eulerian, fixed-grid model has been developed to examine fingering and splashing behaviour during droplet impact against a solid surface. The model employs a volume tracking technique to follow the free surface, and treats surface tension in a continuous manner. Equations are discretized on a Cartesian grid, which unfortunately imposes an unwanted symmetry onto the results. An alternative approach might be to discretize the equations on a cylindrical mesh, but at the expense of limiting the applicability of the model to normal impacts only. Results of two simulations are compared with experiment, and demonstrate the capability of the model to predict fingering and splashing, and to yield reasonable estimates of the number of fingers which form. Results of a third simulation are presented as an example of the grid resolution required as the number of fingers increases. Simulations on finer resolutions are planned.

References

[1] D. B. Kothe and R. C. Mjolsness. RIPPLE: A new model for incompressible flows with surface tension. *AIAA J.*, 30:2694, 1992.

[2] A. M. Worthington. On the forms assumed by drops of liquids falling vertically on a horizontal plate. *Proc. R. Soc. London*, 25:261–271, 1876.

[3] R.F. Allen. The role of surface tension in splashing. *J. Colloid Interface Sci.*, 51(2):350–351, 1975.

[4] H. Marmanis and S.T. Thoroddsen. Scaling of the fingering pattern of an impacting drop. *Phys. Fluids*, 8(6):1344–1346, 1996.

[5] C. D. Stow and M. G. Hadfield. An experimental investigation of fluid flow resulting from the

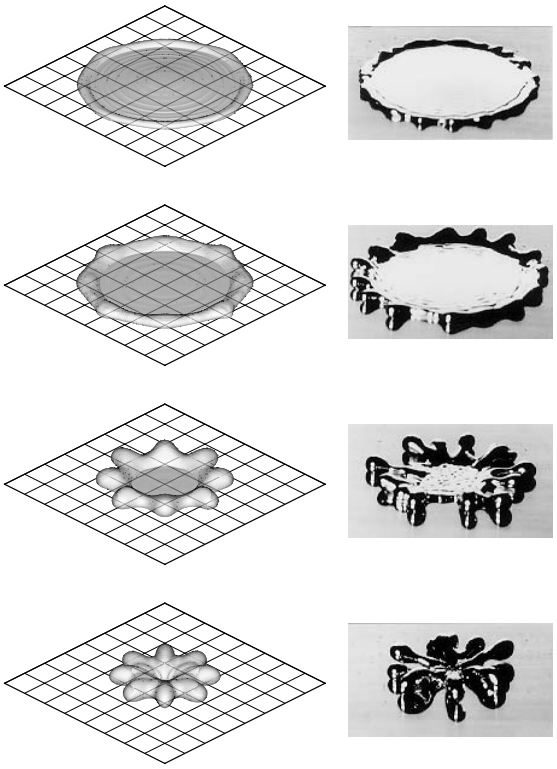

Figure 2: Simulation views and photographs of a 2.7 mm tin droplet impacting at 2 m/s. Results presented at 2, 4, 6 and 7 ms following impact.

impact of a water drop with an unyielding dry surface. *Proc. R. Soc. London A*, 373:419–441, 1981.

[6] C. Mundo, M. Sommerfeld, and C. Tropea. Droplet-wall collisions. Experimental studies of the deformation and breakup process. *Int. J. Multiphase Flow*, 21(2):151–173, 1995.

[7] J. Fukai, Y. Shiiba, T. Yamamoto, O. Miyatake, D. Poulikakos, C. M. Megaridis, and Z. Zhao. Wetting effects on the spreading of a liquid droplet colliding with a flat surface: Experiment and modeling. *Phys. Fluids*, 7:236, 1995.

[8] M. Pasandideh-Fard, Y. M. Qiao, S. Chandra, and J. Mostaghimi. Capillary effects during droplet impact on a solid surface. *Phys. Fluids*, 8(3):650–659, 1996.

[9] J. U. Brackbill, D. B. Kothe, and C. Zemach. A continuum method for modeling surface tension. *J. Comput. Phys.*, 100:335, 1992.

[10] B. van Leer. Towards the ultimate conservative finite difference scheme IV. *J. Comput. Phys.*, 32:101, 1979.

[11] C. S. Peskin. Numerical analysis of blood flow in the heart. *J. Comput. Phys.*, 25:220, 1977.

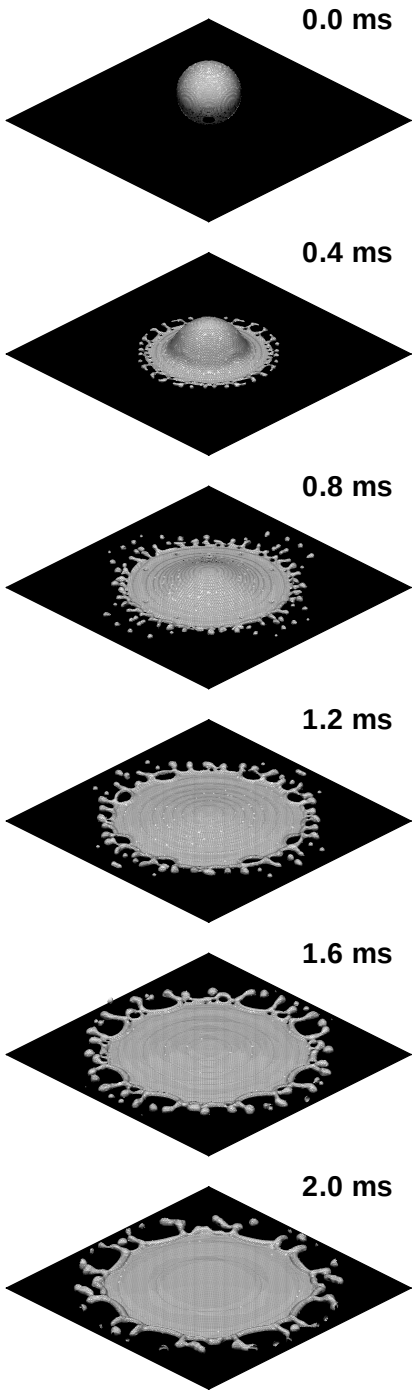

Figure 3: Simulation views of a 2.7 mm tin droplet impacting at 3 m/s. The numbers beside each view indicates the time following impact.

[12] I. Aleinov and E. G. Puckett. Computing surface tension with high-order kernels. In K. Oshima, editor, *Proceedings of the 6th International Symposium on Computational Fluid Dynamics*, pages 13–18, 1995.

[13] D. L. Youngs. An interface tracking method for a 3D Eulerian hydrodynamics code. Technical Report 44/92/35, AWRE, 1984.

[14] M. Pasandideh-Fard, R. Bhola, S. Chandra, and J. Mostaghimi. Droplet impact and solidification: Comparison of experimental and numerical results. In *Proceedings of the 1997 National Heat Transfer Conference*, ASME HTD 347-349, pages 21–29, 1997.

[15] B. J. Daly. Numerical study of two fluid Rayleigh-Taylor instability. *Phys. Fluids*, 10(2):297–307, 1967.

[16] A. Elgowainy and N. Ashgriz. The Rayleigh-Taylor instability of viscous fluid layers. *Phys. Fluids*, 9(6):1635–1649, 1997.